



NLR-TP-2005-470

Stress intensity factors and crack propagation in single crystal nickel based superalloy CMSX-4


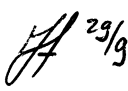
T. Tinga

This report is based on a paper to be submitted to Engineering Fracture Mechanics,
Elsevier Science.

This report may be cited on condition that full credit is given to NLR and the author.

Customer: National Aerospace Laboratory NLR
Working Plan number: AV.1.A - AV.1.B - AV.1.C
Owner: National Aerospace Laboratory NLR
Division: Aerospace Vehicles
Distribution: Unlimited
Classification title: Unclassified
August 2005

Approved by:

Author	Reviewer	Managing department
 29/9/05	 29/9	BO 29/09



Summary

A 3-D finite element method was used to calculate the stress intensity factors for CMSX-4 single crystal corner cracked specimens. The anisotropic material properties and inclinations of the cracks were shown to have significant effects on the stress intensities. Then the 2-D resolved shear stress approach for predicting the crack planes and crack growth directions in single crystals was extended to the 3-D case. Finally the approach was extended to the more complex geometries of actual gas turbine components, for which an efficient crack growth analysis method is proposed, based on the influence function method.



Contents

1	Introduction	5
2	Isotropic and anisotropic stress intensity factors	7
3	Stress intensity factors for single crystal corner cracked specimens	8
	3.3 Angled crack, isotropic properties	12
	3.1.1 <i>(Near) edge positions</i>	12
	3.1.2 <i>(Near) centre position</i>	13
	3.1.3 <i>Angled crack projection approximation</i>	13
	3.4 Angled crack, orthotropic properties	14
4	Resolved shear stress intensity parameter	15
	4.1 Original crack normal to tensile axis, perfect crystallographic alignment	16
	4.2 Original +45° crack, perfect crystallographic alignment	16
	4.3 Original +45° crack, imperfect crystallographic alignment	17
5	Application to single crystal gas turbine components	18
	5.1 Crack propagation analysis constituents	18
	5.1.1 Direction of crack propagation	19
	5.1.2 Fracture mechanics parameters	19
	5.1.3 Method to determine fracture mechanics parameter	19
	5.1.4 Method for crack propagation analysis	20
	5.2 Closed form SIF for complex geometries	20
	5.2.1 Method to determine closed form SIF	21
	5.2.2 Application of the method	23
	5.3 Crack propagation analysis method for single crystal gas turbine components	26
6	Concluding remarks	26
7	Acknowledgements	27
8	References	27

5 Tables
15 Figures

(28 pages in total)



Stress intensity factors and crack propagation in single crystal nickel based superalloy CMSX-4

Tiedo Tinga*

National Aerospace Laboratory NLR, Anthony Fokkerweg 2, 1059 CM, Amsterdam, The Netherlands

Abstract

A 3-D finite element method was used to calculate the stress intensity factors for CMSX-4 single crystal corner cracked specimens. The anisotropic material properties and inclinations of the cracks were shown to have significant effects on the stress intensities. Then the 2-D resolved shear stress approach for predicting the crack planes and crack growth directions in single crystals was extended to the 3-D case. Finally the approach was extended to the more complex geometries of actual gas turbine components, for which an efficient crack growth analysis method is proposed, based on the influence function method.

Keywords: Stress intensity factor; single crystal; anisotropy; CMSX-4 superalloy; gas turbine; influence function method

1 Introduction

To improve gas turbine efficiency the turbine inlet temperatures have steadily increased. This makes greater demands on the materials used for the turbine rotor blades and stator vanes. One way to meet these demands is to use single crystal materials. In modern jet engines single crystal materials are used for the turbine blades and vanes.

As part of component life assessment the material fatigue crack propagation behaviour must be modelled. Two major differences exist for the crack growth analysis of single crystal materials compared to the polycrystalline case. Firstly the material behaviour is anisotropic, which results in different stress and deformation fields around the crack tip. Secondly, cracks

* Corresponding author. Tel.: +31-527-248727; fax: +31-527-248210.
Email address: tinga@nlr.nl



Nomenclature

a, a_{cr}	crack length
a, b, c	material orientation angles in analysis tool
a_{ij}	material constitutive matrix
BE	boundary element
C_{ij}	material constitutive matrix (in FE)
ΔK	stress intensity factor range
E	Young's modulus
FCC	face centred cubic (crystal lattice)
FE	finite element
G	shear modulus / energy release rate
HPT	high pressure turbine
K, K_I, K_{II}, K_{III}	stress intensity factors (modes I, II and III)
K_{eff}	effective stress intensity factor
K_{rss}	resolved shear stress intensity parameter on slip system
LEFM	linear elastic fracture mechanics
r	distance to crack tip
S	remotely applied stress
SIF	Stress Intensity Factor
t	specimen width
T	projected specimen width
α, β	crack orientation angles in analysis tool
β	geometrical correction function for SIF
ε	strain
μ_i	roots of characteristic equation
ν	Poisson's ratio
σ	stress
τ_{rss}	resolved shear stress
θ	angle with respect to the normal crack plane

propagate along distinct crystallographic planes, which means they are often angled cracks not on a plane normal to the major principal stress, unlike cracks in isotropic materials.

To model single crystal crack propagation behaviour the anisotropic stress intensity factors should be determined for both normally-oriented and angled cracks. Many studies have been done on the fracture mechanics of anisotropic materials, both on bulk materials [1-4,9,15] and notched geometries [5,6]. The earlier papers [1-3,9,15] mainly focus on 2-dimensional cases and analytical approaches, whereas the more recent work [5-7,17] directs towards 3-dimensional



cases and numerical methods. However, still anisotropic stress intensity factor solutions are usually not available. Therefore it has often been assumed, or shown for specific materials [1,2,4], that the differences between isotropic and anisotropic solutions are negligible and that the isotropic solution can be used. Similarly, it has been assumed [2,4] that the standard stress intensity factor solutions for normally-oriented cracks can be used for angled cracks, provided the angles made with the normal plane are small.

The first objective of the present work is to show that standard stress intensity factor solutions cannot be used for the anisotropic CMSX-4 and angled cracks. The second objective is to extend to 3 dimensions the 2-dimensional resolved shear stress method [1,3,4,8] for predicting the crack planes and crack growth directions in single crystals. The final objective is to develop a method for the analysis of crack growth in complex geometries of real gas turbine components, which translates the work to an engineering level.

2 Isotropic and anisotropic stress intensity factors

The basis of linear elastic fracture mechanics (LEFM) theory is the stress intensity factor (SIF or K) concept, which relates the local elastic stress field near the crack tip to the known global stress or displacement field. Relations for the stress intensity factor can be derived by calculating the stress or displacement field as functions of the distance r and angle θ , see Figure 1. The stress field in a small region surrounding the crack tip is given by [9,10]

$$\sigma_{ij}(r, \theta) = \frac{1}{\sqrt{2\pi r}} [K_I f_{ij}(\mu, \theta) + K_{II} g_{ij}(\mu, \theta) + K_{III} h_{ij}(\mu, \theta)] \quad (i, j = 1, \dots, 6) \quad (1)$$

In this relation f_{ij} , g_{ij} and h_{ij} are geometrical functions defining the angular dependency of the stress field, and K_I , K_{II} and K_{III} are the mode I, II and III stress intensity factors. For the anisotropic case the stress field also depends on the root μ of the characteristic equation, which is defined below. In an infinite plate containing a crack with length $2a$ and loaded by a normal stress σ_{yy} and shear stresses τ_{xy} and τ_{yz} , the stress intensity factors are defined as

$$K_I = \sigma_{yy} \sqrt{\pi a} \quad ; \quad K_{II} = \tau_{xy} \sqrt{\pi a} \quad ; \quad K_{III} = \tau_{yz} \sqrt{\pi a} \quad (2)$$

For any situation deviating from this ideal situation the value of K is modified by a factor $\beta(a)$, e.g.:

$$K_I = \sigma_{yy} \sqrt{\pi a} \cdot \beta_I(a) \quad (3)$$

The function $\beta(a)$ accounts for geometrical effects like finite width corrections. A number of handbooks are available [11,12] in which the function $\beta(a)$ is supplied for most common problems, but it can also be obtained from a finite element (FE) analysis by comparing the calculated displacement field (which in an FE analysis is more accurate than the stress distribution) with the (theoretical) displacement field around a crack in an infinite plate loaded in plane tension.

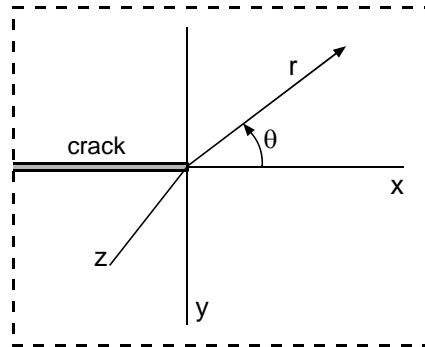


Figure 1 Definition of crack tip coordinate frame

For isotropic materials the functions f_{ij} , g_{ij} and h_{ij} can be related directly to the material properties E and ν , but for anisotropic materials, they are functions of the complex roots μ_i of the characteristic equation [9]

$$a_{11}\mu^4 - 2a_{16}\mu^3 + (2a_{12} + a_{66})\mu^2 - 2a_{26}\mu + a_{22} = 0 \quad (4)$$

where the coefficients a_{ij} are the (compliance) elements of the elastic constitutive matrix, relating the stresses and strains according to

$$\varepsilon_i = a_{ij}\sigma_j \quad (i, j = 1, \dots, 6) \quad (5)$$

This constitutive matrix must be defined in the coordinate frame of the crack (see Figure 1).

In the next section we describe how an FE analysis is used to calculate the anisotropic stress intensity factors for single crystal corner cracked specimens of a nickel-base superalloy.

3 Stress intensity factors for single crystal corner cracked specimens

The commercial finite element code MSC.Nastran was used to calculate the stress intensity factors for single crystal corner cracked specimens of a nickel-base superalloy. MSC.Nastran provides special crack tip elements (CTEs), whose midside nodes are moved to the quarter positions to better represent the stress field singularity at the crack tip. The calculated stress intensity factors are directly given as element output.

The NLR in-house tool *NLR-C3D* [13] was used to insert an initial crack in an existing finite element model. *NLR-C3D* replaces elements in the mesh by crack blocks, which define the crack plane and locally refine the mesh, see

Figure 2. It also inserts the CTEs, six (6) along the crack front in the present case, and automatically calculates stress intensity factors for different crack sizes.

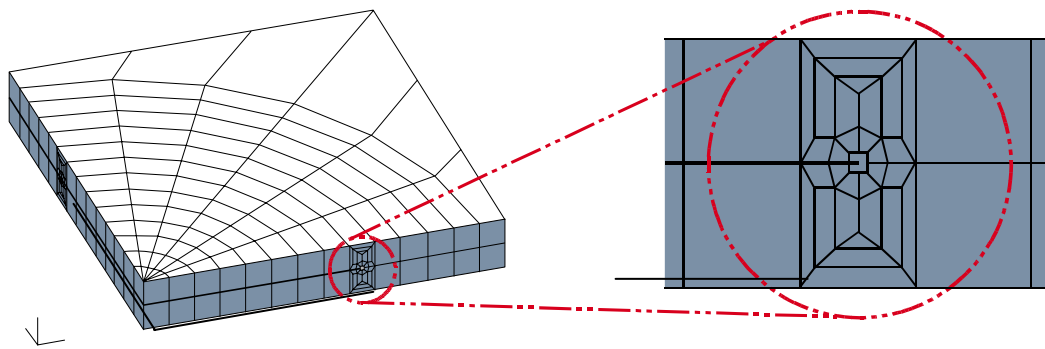


Figure 2 Slice of FE model near the crack plane and detailed view of crack blocks inserted by NLR-C3D tool

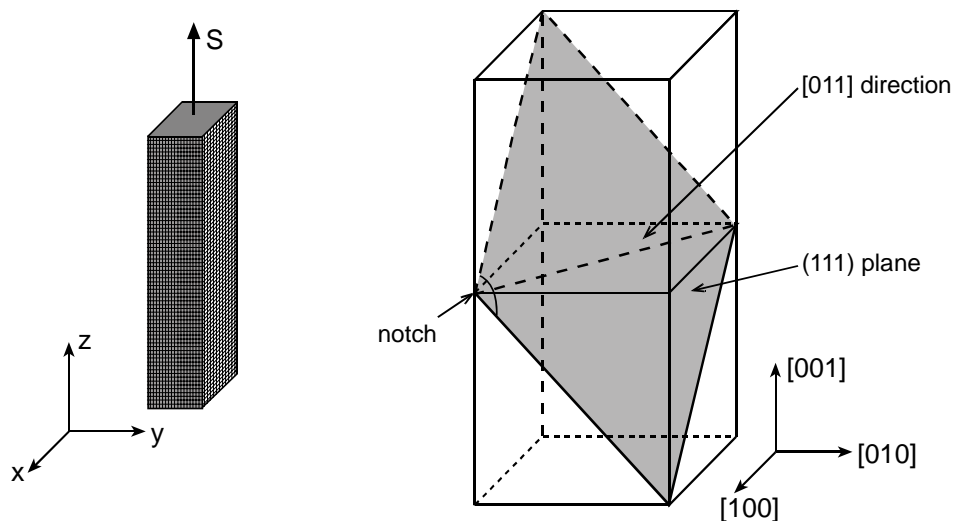


Figure 3 Schematic representation of crystal orientation in test specimen and important crystal directions and planes

Stress intensity factors were calculated for two cases: a corner crack propagating on the plane normal to the applied load, and a corner crack propagating on a 45° plane as shown in Figure 3. The latter case represents the situation in which a crack propagates along a $\{111\}$ -type plane in a single crystal FCC material aligned with the $[001]$ direction along the tensile axis (z -axis), and the $[100]$ and $[010]$ directions along the x - and y -axes. Since corner cracks are 3-dimensional, the stress intensity factor (SIF) solutions were calculated for six (6) different positions along the crack fronts, corresponding to the angular centres of each CTE. The two FE meshes are shown in Figure 4. These are somewhat more detailed than the meshes used by Pickard [10].

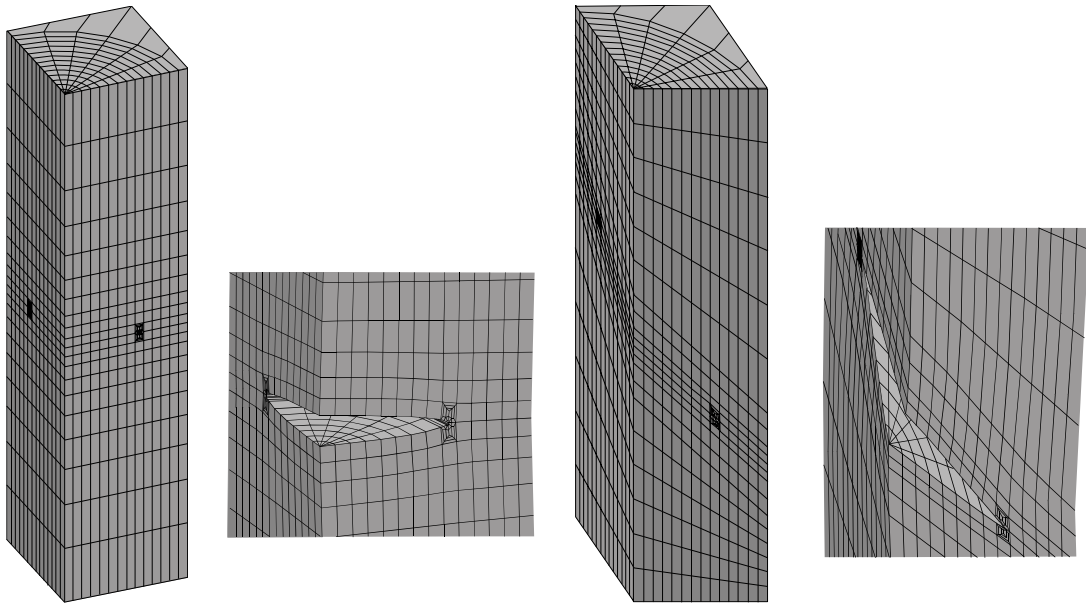


Figure 4 Finite element models for corner cracked specimen with a crack normal to the tensile axis (left) and a crack under a 45° angle (right)

To quantify the effect of material anisotropy on the stress intensity factors, the SIF values for both the normal and 45° angled cracks were calculated with isotropic and anisotropic material properties, see Table 1.

Table 1 Material properties for Ni-based superalloy

Property	Isotropic	Orthotropic
E	200 Gpa	200 GPa
ν	0.30	0.30
G	76.9 Gpa	220 GPa
a_{11}	5.00E-12 Pa ⁻¹	5.00E-12 Pa ⁻¹
a_{12}	-1.50E-12 Pa ⁻¹	-1.50E-12 Pa ⁻¹
a_{14}	1.30E-11 Pa ⁻¹	4.55E-12 Pa ⁻¹

3.1 Normal crack, isotropic properties

The FE model was checked by calculating the corner crack mode I SIFs for a normal crack in an isotropic material and comparing them to the solutions given by Pickard [10] and in an AGARD publication [14]. Figure 5a shows the comparisons for SIFs along the specimen edges (actually 7.5° from the specimen edges for the MSC.Nastran results): the agreement is generally good to excellent.

Figure 5b compares the edge and centre position SIFs according to Pickard's FE model and the present one. Both models predict higher SIFs along the specimen edges. This difference

can be explained by the fact that edge positions are nominally in plane stress, whereas the centre position is nominally in plane strain.

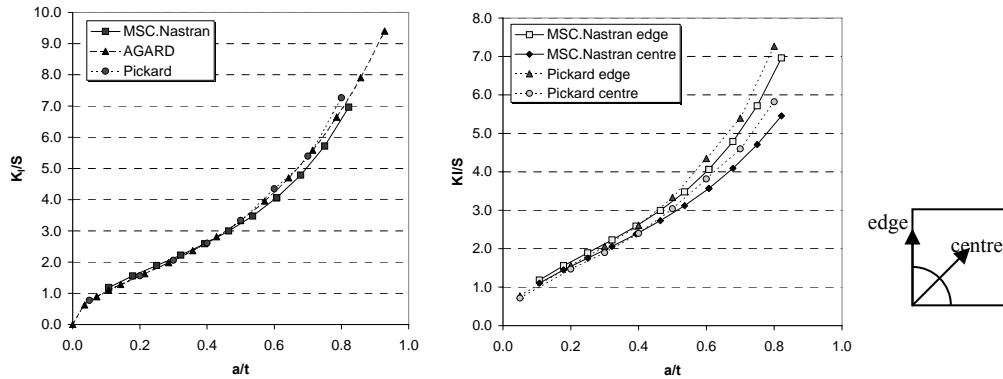


Figure 5 K_I for normal crack and isotropic material: a) comparison of edge solutions and b) showing the difference between a centre and edge position on the crack front

3.2 Normal crack, orthotropic properties

Figure 6 shows that changing the material properties from isotropic to anisotropic, in the present case orthotropic, more than doubles the K_I values for the normal crack orientation. Also, the difference in K_I between the edge and centre positions is almost the same (factor ~ 1.3) for both isotropic and orthotropic properties. This is worth noting because in the orthotropic case the elastic properties in the near- $\langle 100 \rangle$ directions associated with the crack edge (7.5°) positions are different from those for the near- $\langle 110 \rangle$ directions associated with the crack centre ($37.5^\circ, 52.5^\circ$) positions.

There are two ways in which material anisotropy can affect the value of the stress intensity factor. Firstly, just using the anisotropic method influences the SIF. Secondly, the material anisotropy changes the local stress distribution, which also affects the SIF. Snyder and Cruse [15] concluded that the first effect is quite small (comparing isotropic or anisotropic solutions in the same stress field), but the second effect is much larger. This second effect is automatically included when SIFs are calculated with an FE method, and so Snyder's and Cruse's conclusion is confirmed by the results in Figure 6.

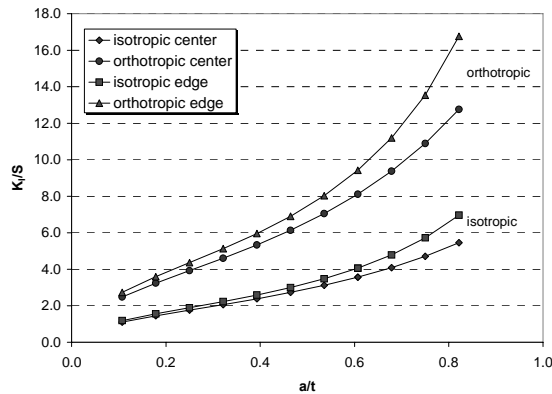


Figure 6 K_I for normal crack, using isotropic and orthotropic material properties

3.3 Angled crack, isotropic properties

The MSC.Nastran stress intensity factors for an angled crack in an isotropic material are compared with the results of Pickard [10] in Figures 7a and 7b for edge and centre positions, respectively, and are discussed in the following paragraphs:

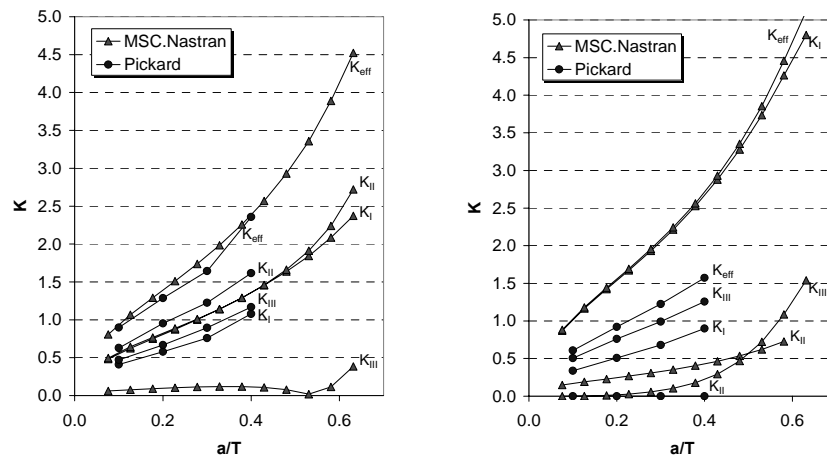


Figure 7 SIF solutions for 45° angled crack: a) for an edge position (7.5°), b) for a centre position (37.5°, 52.5°): note that the abscissa is a/T , where $T = t$ for a normal crack and $T = t\sqrt{2}$ for a 45° crack

3.1.1 (Near) edge positions

For the edge positions, Figure 7a, the crack plane is at 45° to the tensile axis, which means that both mode I and mode II loading are present, with the same magnitude, but mode III is absent. Therefore one expects similar K_I and K_{II} values and negligible K_{III} . This is the case for the MSC.Nastran results. However, Pickard's data show clear differences between K_I and K_{II} and significant K_{III} values. These results are hard to explain. They may be due to differently applied boundary conditions, which resulted in the specimen deforming in a less defined way.



On the other hand, the values of K_{eff} , which is the overall driving force for crack growth on the angled plane, and is defined for isotropic materials by

$$K_{eff} = \sqrt{K_I^2 + K_{II}^2 + K_{III}^2} \quad (6)$$

are fairly similar for the MSC.Nastran and Pickard solutions.

3.1.2 (Near) centre position

For the centre position it can be seen from

Figure 3 that the crack propagates in a direction normal to the tensile axis but on a plane tilted 45° . Thus the loading is basically mode I, but with a mode III (tearing load) contribution. One would therefore expect similar K_I values for normal and angled cracks: comparison of the lowest curve in Figure 6 with the uppermost curve in Figure 7b shows that this is indeed the case.

Furthermore, K_{II} should be negligible and K_{III} should be non-zero. The MSC.Nastran results in Figure 7b do not agree well with these expectations. The most likely reason is the use of only six CTEs, which means that K values are obtained for near centre (37.5° , 52.5°) positions rather than the exact centre (45°). At the 45° position K_{II} does become zero [10], while K_{III} reaches a maximum there. For the MSC.Nastran results, the K_{II} -values at 37.5° and 52.5° have similar values but opposite sign, so interpolation yields $K_{II} = 0$ at 45° .

Pickard's results in Figure 7b are again hard to explain, especially the K_I curve, which is much lower than the MSC.Nastran K_I curve. As a result, also the K_{eff} curves show a large difference in this case.

3.1.3 Angled crack projection approximation

It is often suggested to approximate the SIFs for an angled crack by using the normal crack SIF solution with the *projected* crack length, i.e. the apparent length of an angled crack when it is projected onto the normal plane. Figure 8 shows that this approximation is invalid for an edge position of a 45° crack, whether one compares the normal crack K_I ($= K_{eff}$) curve with the angled crack K_I or K_{eff} curves. A similar result will be obtained for the centre position.

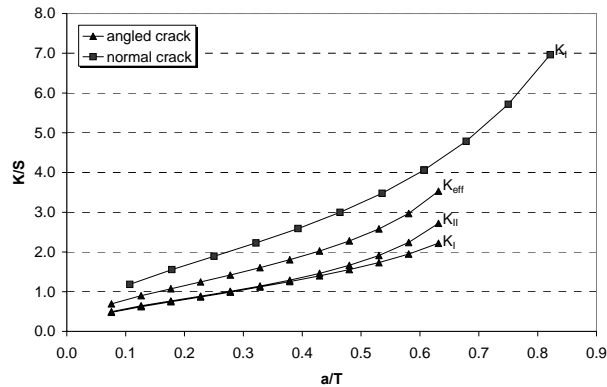


Figure 8 Comparison between normal crack and 45° angled crack for an edge position: note that the abscissa is a/T , where $T = t$ for a normal crack and $T = t\sqrt{2}$ for a 45° crack

3.4 Angled crack, orthotropic properties

The calculated results for the angled crack, using orthotropic material properties are shown in Figure 9. It appears from Figure 9a that for an edge position the effect of using orthotropic instead of isotropic properties leads to different SIF solutions, especially for K_{II} . However, both K_I and K_{II} are lower for the orthotropic case, whereas for a normal crack Figure 6 shows that the orthotropic K_I is significantly greater. Figure 9b shows that for a centre position the difference between orthotropic and isotropic stress intensity factors is smaller, especially for K_{II} , but the trends are the same as for an edge position.

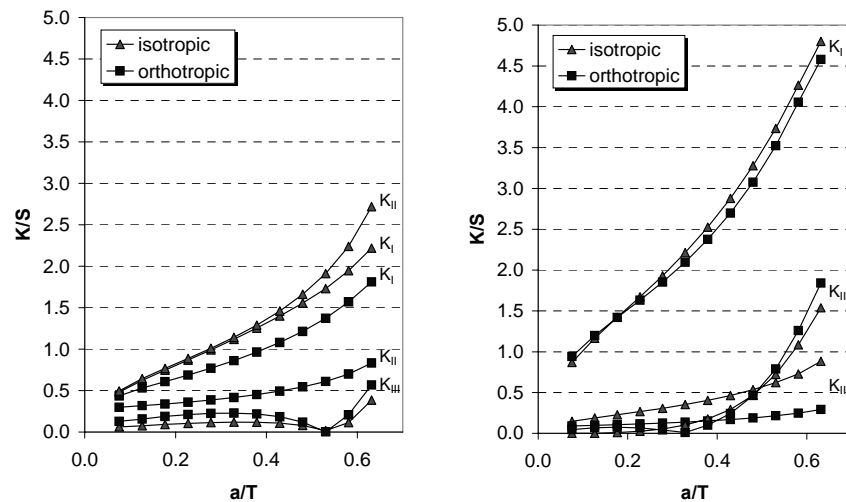


Figure 9 SIF solutions for 45° angled crack. Comparison between isotropic and orthotropic properties for a) edge position and b) centre position: note that the abscissa is a/T , where $T = t$ for a normal crack and $T = t\sqrt{2}$ for a 45° crack

4 Resolved shear stress intensity parameter

The crack planes and propagation directions in single crystals cannot be predicted from the stress field alone, since cracking is restricted to distinct crystallographic planes. Telesman and Ghosn [1] and Chen and Liu [3] presented a 2-dimensional prediction method based on a resolved shear stress intensity parameter that represents the stress intensity on a specific crystallographic plane. The resolved shear stress intensity parameter is defined as

$$K_{r_{ss}} = \lim_{r \rightarrow 0} \tau_{r_{ss}} \sqrt{2\pi r} \quad (7)$$

where the value of $\tau_{r_{ss}}$ is obtained by Schmid-decomposition of the stress tensor to a specific slip system. The limiting value of $K_{r_{ss}}$ is obtained by calculating several values near the crack tip and extrapolating to $r = 0$. Crack propagation will occur on the slip plane with the highest value of $K_{r_{ss}}$.

As stated in section 2, calculations of SIF values with an FE method are most accurate when they are based on displacements. However, a displacement vector cannot be projected to a slip system. to obtain the resolved shear stress. Telesman and Ghosn [1] calculated $K_{r_{ss}}$ from a 2-dimensional reconstructed stress field around the crack tip of an isotropic material, using a boundary integral equation method.

In the present work the stress tensor was reconstructed from the 3-dimensional anisotropic (orthotropic) FE calculations of SIF values for specific situations, together with equation (1). Use of equation (1) requires choosing values of θ . The most obvious choice is the angle between the slip plane (*possibly* destined to become the new crack plane) and the plane normal to the tensile axis, as was done by Telesman and Ghosn [1].

The $K_{r_{ss}}$ calculation was incorporated into an analysis tool that requires the following information:

- (1) The elastic properties (E , G and ν for the $\langle 100 \rangle$ cube directions) of the material.
- (2) SIF values (K_I , K_{II} and K_{III} for the appropriate orthotropic material and crack orientation) at certain crack lengths.
- (3) The crystallographic orientation of the material with respect to the specimen coordinate frame. This is specified by three angles (a , b and c), which define the rotation around the specimen x -, y - and z -axes, respectively.
- (4) The orientation of the original crack plane with respect to the specimen coordinate frame. This is specified by another two angles (α and β), which define the rotation of the crack plane around the specimen x - and y -axes.

The analysis tool then calculates $K_{r_{ss}}$ for every slip plane and finds the maximum value. The corresponding slip plane then determines the plane and directions of subsequent crack growth. This can be done for any material orientation and any crack orientation.

More specifically, for the present work the analysis tool was used to predict the planes and directions of crack propagation in the corner cracked specimens described in section 3. The predictions are compared in subsections 4.1-4.3 with representative experimental results for fatigue crack growth in single crystal CMSX-4 specimens [16].

4.1 Original crack normal to tensile axis, perfect crystallographic alignment

When the original crack plane is normal to the tensile axis ($\alpha = \beta = 0$) and the crystallographic alignment of the specimen is perfect ($a = b = c = 0$) there are four slip systems with the same K_{rss} . This is illustrated in Table 2 for an arbitrary original crack length of 1.5 mm: the K_{rss} value of 1.30 for the Edge 1 position shows that subsequent crack propagation is likely at both -45° and $+45^\circ$ to the tensile axis. The first column in Table 2 specifies the position along the original crack front.

Table 2 Originally normal crack ideal situation ($a = b = c = 0, \alpha = \beta = 0, a_{cr} = 1.5 \text{ mm}$)

Position	K_{rss}	Active slip systems	Subsequent crack angle
Edge 1	1.30	(111)[0 $\bar{1}$ 1], (1 $\bar{1}$ $\bar{1}$)[01 $\bar{1}$]	-45°
	1.30	(1 $\bar{1}$ 1)[011], (11 $\bar{1}$)[0 $\bar{1}$ $\bar{1}$]	$+45^\circ$
Centre	1.47	(111)[0 $\bar{1}$ 1]	-54.7°
	1.47	(11 $\bar{1}$)[0 $\bar{1}$ $\bar{1}$]	$+54.7^\circ$
Edge 2	1.30	(111)[0 $\bar{1}$ 1], (1 $\bar{1}$ 1)[011]	-45°
	1.30	(1 $\bar{1}$ $\bar{1}$)[01 $\bar{1}$], (11 $\bar{1}$)[0 $\bar{1}$ $\bar{1}$]	$+45^\circ$

4.2 Original $+45^\circ$ crack, perfect crystallographic alignment

In this second example the original crack was at $+45^\circ$ to the tensile axis. Starting with an edge length of only 0.1 mm, the predictions were that the crack stays on the original slip plane until at least 0.5 mm length. This is shown in the first row of Table 3. However, when the crack becomes larger than 0.5 mm it is predicted to switch to the -45° slip plane, see the second row in Table 3.

Table 3 Originally $+45^\circ$ angled crack ($a = b = c = 0, \alpha = 45^\circ, \beta = 0$)

Position	K_{rss}	Active slip systems	Subsequent crack angle
Edge 1 - $a_{cr} = 0.5 \text{ mm}$	0.655	(1 $\bar{1}$ 1)[011]	$+45^\circ$
Edge 1 - $a_{cr} = 0.6 \text{ mm}$	0.621	(111)[0 $\bar{1}$ 1]	-45°

After some amount of crack growth, the same process will cause the crack to switch back to the $+45^\circ$ slip plane. In fact, what actually happens is that a crack grows in a zig-zag fashion, alternating between $+45^\circ$ and -45° and remaining macroscopically in the plane normal

to the tensile axis. This was observed for specimen A of the experimental programme [16], see figure 10a, although the alignment for this specimen was not perfect. This is discussed further in subsection 4.3.

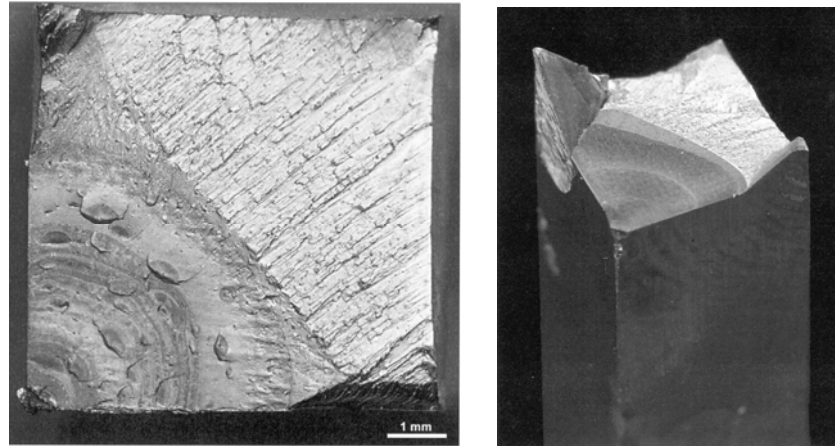


Figure 10 a) fracture surface in corner cracked specimen A. The crack front is macroscopically normal to the tensile axis. b) specimen B fracture surface, showing the transition from normal to angled crack plane. Both photographs from [Ref.11]

4.3 Original +45° crack, imperfect crystallographic alignment

If the crystallographic alignment of the specimen is imperfect, there should be a preference for crack growth on one slip plane. Then, since the crack does not switch to another slip plane, a macroscopically angled crack develops.

Using the K_{RSS} approach the misalignment behaviour was analysed for a +45° original crack and five simple crystallographic misalignments, whereby $a = 3^\circ, 5^\circ, 7^\circ, 10^\circ, \text{ and } 15^\circ$, and $b = c = 0$. Starting with an edge crack length of 0.1 mm, the predictions were that all cracks stay on the original slip plane until lengths of 1.1 - 4.5 mm, depending on the misalignment, see Table 4. These crack lengths are significantly larger than the 0.5 mm for a perfectly aligned specimen (see Table 3) and as the misalignment increases there is eventually no change of slip plane.

This means that the crack grows in a zig-zag fashion until the crack length is reached where no transition to another slip plane is possible anymore. Table 4 shows that for small misalignments ($a \sim 3^\circ - 5^\circ$) there is no such crack length and for large misalignments ($a \sim 10^\circ - 15^\circ$) this crack length is zero, indicating that an angled crack develops from the beginning. For intermediate misalignments there is a crack length at which the crack switches, but there is also a length above which no switching can occur anymore.



Table 4 Crack lengths at which preferred direction changes from $+45^\circ$ to -45° for different material orientations ($b = c = 0$, $\alpha = 45^\circ$, $\beta = 0$)

Position	$a = 3^\circ$	$a = 5^\circ$	$a = 7^\circ$	$a = 10^\circ$	$a = 15^\circ$
Edge 1	1.4 mm	2.2 mm	4.5 - 6.5 mm ^a	no change	no change
Edge 2	0.0 mm	1.1 mm	1.6 - 3.7 mm ^a	2.1 - 3.3 mm ^a	no change

^a preferred direction changes to -45° at first crack length, but is again $+45^\circ$ for cracks larger than the second crack length (= no subsequent change beyond this crack length).

Thus a macroscopically normal crack can develop in two situations:

- (1) Perfect crystallographic alignment: a zig-zag crack develops because switching is not bounded by a certain crack length.
- (2) Intermediate misalignment: the bounding crack length at which the zig-zag crack transitions into an angled crack is beyond the crack length at failure.

The data in Table 4 enable explaining the fatigue crack growth behaviour of the specimens shown in Figure 10. Specimen A had a primary crystallographic misalignment of 8.5° and also a considerable secondary misalignment of $c = 8^\circ$ [16]. Crack growth occurred in a zig-zag fashion, Figure 10a. This is an example of an intermediate misalignment with a transition to an angled crack beyond the crack length at failure. However, specimen B had a primary misalignment $a = 7.3^\circ$ and only a slight secondary misalignment. This resulted in one transition from the normal crack plane to an angled crack plane at an edge crack length of 3.8 mm, see the L.H. edge in Figure 10b. The transition crack lengths agree reasonably with the predictions in Table 4.

5 Application to single crystal gas turbine components

Although the corner cracked specimen is a simple geometry, the approach in the present work is based on finite element analyses. This means that it can be extended to the more complex geometries of actual gas turbine components (single crystal turbine blades and vanes). In this section the constituents of a crack growth analysis and an efficient method to do the analysis on a geometrically complex single crystal component are discussed and proposed.

5.1 Crack propagation analysis constituents

A crack propagation analysis relates a load sequence in terms of a fracture mechanics parameter to the material crack growth behaviour. A wide range of approaches for such analyses has been developed, as reviewed by Timbrell et al. [17]. Depending on the application, choices are made for the following four constituents:

- (1) A criterion for the direction of crack propagation.



- (2) A fracture mechanics parameter representing the load sequence.
- (3) A method to determine the fracture mechanics parameter.
- (4) A method to calculate the crack propagation as a function of number of cycles.

These constituents will be discussed separately in the next subsections, and the choices for the method proposed in the present work will be motivated.

5.1.1 Direction of crack propagation

The direction of crack propagation is generally assumed to be the direction normal to the maximum principal stress or the direction of maximum energy release rate. In the previous sections it was shown that for single crystal materials the maximum value of K_{rss} is a suitable criterion to determine the direction of crack propagation. This parameter will therefore be used.

5.1.2 Fracture mechanics parameters

The primary fracture mechanics parameters of interest for crack propagation are the stress intensity factor K and the energy release rate G . A complication of the stress intensity factor is the division into three modes, represented by K_I , K_{II} and K_{III} . In complex 3D geometries mixed mode loading often occurs, which means that the three values of K_I , K_{II} and K_{III} must be combined into one *effective* loading parameter. Equation (6) is often used to calculate K_{eff} for isotropic materials [2,4], whereas K_{rss} is the most appropriate quantity for single crystal materials.

To avoid the complexity of three different modes, many analysis codes use the energy release rate G as fracture mechanics parameter. However, this needs frequent numerical recalculation of G during the analysis, since it cannot be obtained in closed form. Moreover, material crack growth curves are generally presented in terms of ΔK . If the stress intensity factor is used in the growth analysis, these curves can be applied directly. When the energy release rate is used the data must be transformed, which is inconvenient and a source of additional inaccuracy.

In the proposed approach the stress intensity factors K_I , K_{II} and K_{III} will be used as fracture mechanics parameters, since they can be used to calculate K_{rss} .

5.1.3 Method to determine the fracture mechanics parameter

There are three main numerical approaches to provide the stress intensity factors:

- (1) Closed form solution.
- (2) Boundary element method.
- (3) Finite element method.

In the closed form approach a known solution provides stress intensity factors as functions of geometry, crack size and loading. These solutions may be derived from analytical expressions or interpolated from results obtained using boundary element or finite element



methods. They are available from several handbooks [10-12]. The main advantage of this approach is that it provides a potentially fast method to calculate crack propagation, since no complex analysis is required to determine the stress intensity factors for each change in crack length or loading. However, the approach also has limitations. The number of cases for which a solution is available is limited, and load redistribution is not accounted for as the crack grows.

The boundary element (BE) and finite element (FE) methods allow for the analysis of almost any combination of geometry and loading. The main advantage of the boundary element method is that only the boundary of the structure needs to be discretised. The finite element method requires discretisation of the complete structure, but this is compensated for by great flexibility in terms of overall analysis capabilities. In contrast to the closed form approach, using BE or FE methods requires recalculation of the stress intensity factors or energy release rate at each change of crack length or loading.

In the current work it is proposed to calculate the stress intensity factor solution in closed form using the finite element method in combination with the influence function method. This is described in section 5.2.

5.1.4 Method for crack propagation analysis

Finally a method must be chosen to perform the actual crack propagation analysis. There are basically two approaches. In the first approach the calculation of the stress intensity factor and the actual crack propagation analysis are separated. This requires the stress intensity factor to be available in closed form. The actual crack propagation analysis is then very fast, which enables a cycle-by-cycle analysis of the load sequence and the use of advanced (empirical) crack growth models.

In the second approach the crack propagation analysis is integrated in the calculation of the stress intensity factor or the energy release rate in a BE or FE method. Since the fracture mechanics parameter is not available in closed form, it must be calculated again for every analysis step. The associated computation time prohibits the cycle-by-cycle analysis of the load sequence, which is replaced by a block-type analysis. This also prohibits the use of advanced crack growth models. These two facts decrease the accuracy of an analysis following the second approach.

Therefore in the present work the first approach of separated calculation of stress intensity factor and actual crack propagation analysis is chosen.

5.2 Closed form SIF for complex geometries

Use of a closed form stress intensity factor solution is feasible for a complex 3D geometry only if two conditions are fulfilled:



- (1) The stress intensity factor solution can be determined for an arbitrary loading condition and is representative for any loading condition that can possibly occur during the crack propagation analysis.
- (2) The stress intensity factor solution can be scaled by the value of the 3D stress tensor at a uniquely defined location near the crack.

In this subsection, firstly a method to determine the closed form SIF is proposed, and the two conditions are checked. Secondly the method is demonstrated with two examples.

5.2.1 Method to determine closed form SIF

It is readily deduced from the definition of the stress intensity factor K that the values of the three SIFs depend on one single stress tensor component only [11]. Using the crack orientation as defined in Figure 1, these dependencies are given by

$$\begin{aligned}
 K_I &\leftrightarrow \sigma_{yy} \\
 K_{II} &\leftrightarrow \sigma_{xy} \\
 K_{III} &\leftrightarrow \sigma_{yz}
 \end{aligned} \tag{8}$$

For the value of the SIF it is irrelevant which remote loading condition causes the stress state. Therefore, if a normalised stress intensity factor solution (e.g. K_I/σ_{yy}) is calculated using an arbitrary loading condition, this solution is representative for any loading condition, as will be shown in the next subsection. The value of K can be obtained by scaling with the actual stress. This fulfils the first condition.

The location of the stress tensor used for normalising and scaling the SIF solution is subject to two more or less contradictory requirements:

- (1) The location must be outside the region that is affected by the redistribution of the stress field around the crack.
- (2) The location must be close to the crack to be representative for the loading of the crack, especially in a strongly non-uniform stress field as is often present in a 3D component.

From the principle of superposition, as illustrated in Figure 11, it can be shown that the stress distribution along the virtual crack in the *uncracked* model is representative for the loading of the crack and thus quantifies the stress intensity factor. The three problems in

Figure 11 are:

- (a) An uncracked elastic body subjected to a remote external load σ and a body force (F_x, F_y),
- (b) A cracked elastic body subjected to the same external load and body force,
- (c) A cracked elastic body of the same configuration loaded along the cracked surface by a distributed stress which is equal to the stress distribution along the virtual crack surface in (a) required to keep the (virtual) crack closed.

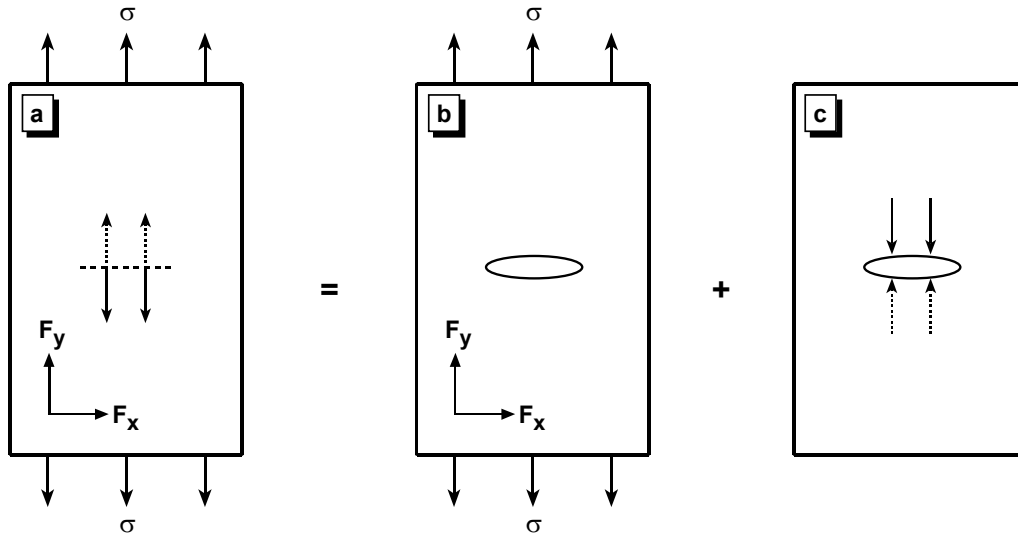


Figure 11 Principle of superposition applied to the crack problem

Since $K = 0$ for problem (a), the values of K for problems (b) and (c) must have equal values but opposite signs. Therefore, changing the sign of the stress distribution in (c) yields exactly the K of problem (b). Further, the stress distribution required to keep a (virtual) crack in problem (a) closed is equal to the stress distribution that is normally present in the body, but again with opposite sign and thus exactly equal to the changed distribution in (c). That proves that the stress distribution at the virtual crack in the *uncracked* and remotely loaded body is representative for the stress intensity factor in the cracked and remotely loaded body. Since no actual crack is present, the first requirement for the location of the stress tensor is automatically satisfied.

For some problems a location close to the crack can be selected to satisfy the second requirement. But for a non-uniform stress field the loading of the crack faces is also non-uniform and therefore cannot be represented by the stress tensor in a single location. The variation of the stress along the crack faces must be taken into account.

The influence function method proposed by Shiratory et al. [18] and applied by Yamashita et al. [19] was used to solve this problem. The relative influence of the stresses at the different parts of the crack face were originally taken into account using the following relation

$$K = \sum_{i=1}^N K_i \sigma_i \quad (9)$$

where σ_i is the nodal stress at the i -th node along the crack face (due to superposition equal to the stress at the virtual crack face in the *uncracked* body, see

Figure 11), K_i is the influence coefficient of the i -th node, and N is the total number of nodes along the crack faces. The influence coefficient K_i is the stress intensity factor of the same crack acted upon by a unit load in the i -th node only. The method is modified slightly to obtain an



expression for effective stress, which can be used to normalise and scale the SIF. Therefore the influence coefficients in equation (9) were normalised and used as weights in the calculation of the effective stress:

$$\sigma_{eff} = \sum_{i=1}^N \left(\frac{K_i}{\sum_j K_j} \right) \sigma_i \quad (10)$$

This effective stress is then used to normalise and scale the value of K , which fulfils the second condition for a closed form SIF.

Whereas in [18] and [19] an influence coefficients database for a limited number of standard problems was used, in the present work the coefficients were calculated by the FE method. This expands the applicability of the method significantly because there is no limitation to standard problems anymore. On the other hand, the computational effort is increased somewhat, because N influence coefficients must be calculated for a series of crack lengths for the problem in hand.

For some special cases the influence function method can be reduced to an even simpler method. For relatively small crack lengths all influence coefficients K_i are very similar and can be assumed to be equal, which means that the effective stress equals the average stress along the crack faces. If, in addition, the loading is also uniform, the nodal stresses will also become very similar and then $\sigma_{eff} = \sigma_i$. In those cases, as an engineering approach, the average stress in the uncracked model or even the stress tensor at only one location (e.g. near the virtual crack tip) can be used to normalise and scale the SIF.

5.2.2 Application of the method

To demonstrate that the stress intensity factor solution determined in this way is representative for any loading condition, two examples were used. Firstly it is shown that the standard SIF solution for an edge crack in a finite width sheet under a bending load can be obtained from the solution of the sheet under a uniaxial tensile stress. Secondly, the feasibility of the method is demonstrated on an FE model of a high pressure turbine blade.

For a simple geometry like the finite width sheet shown in Figure 12 the stress distribution in the uncracked sheet can be calculated analytically. The sheet under tensile loading was used to determine the SIF solution. By using a uniform stress of 100 MPa, the values of K_I for a range of crack lengths were obtained from a handbook [11] and normalised by the applied stress, as shown in Table 5.

For the sheet under bending, with an applied moment of 1 MNm, the bending stress and the average stress on the crack face were calculated and finally the normalised SIF solution was scaled by the average stress to obtain the K_I values for the bending case.

The calculated values were plotted in Figure 13 together with the K_I -values for the bending case as obtained from [11]. Comparison of the results shows that for this configuration the engineering approach of using the average stress is valid for crack lengths smaller than 5

mm ($a/b < 0.5$). Figure 13 also shows the SIF values calculated by the influence function method (IFM) for three crack lengths. This shows that the IF method also provides accurate results for larger crack lengths. The relatively large deviation for the value at 3.5 mm is caused by the coarse FE mesh that was used and the resulting small number of influence coefficients (small N in equation (9)).

Table 5 SIF solution for bending case obtained from tensile case

crack length (mm)	0.01	0.2	0.5	1	2	3	4	5	6	7
σ_{tensile} (MPa)	100	100	100	100	100	100	100	100	100	100
K_I / σ (tensile)	0.006	0.09	0.14	0.21	0.34	0.51	0.75	1.13	1.76	2.82
σ_{bending} (MPa)	600	576	540	480	360	240	120	0	-120	-240
average σ_{bending}	600	588	572	540	480	420	360	300	240	180
K_I (bending)	3.77	52.2	81.2	113.4	165.2	214.7	269.7	338.0	416.0	507.2

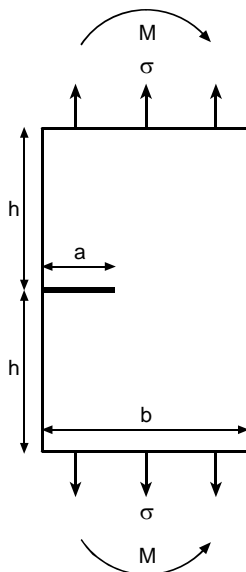


Figure 12 Edge crack in a finite width sheet, loaded by a uniaxial tensile stress (σ) or bending moment (M).
 $b = h = 10$ mm

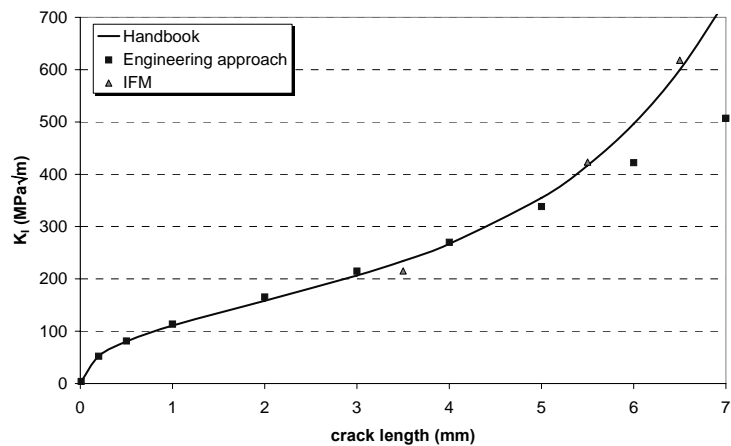


Figure 13 SIF values calculated by IFM and engineering approach compared to handbook values

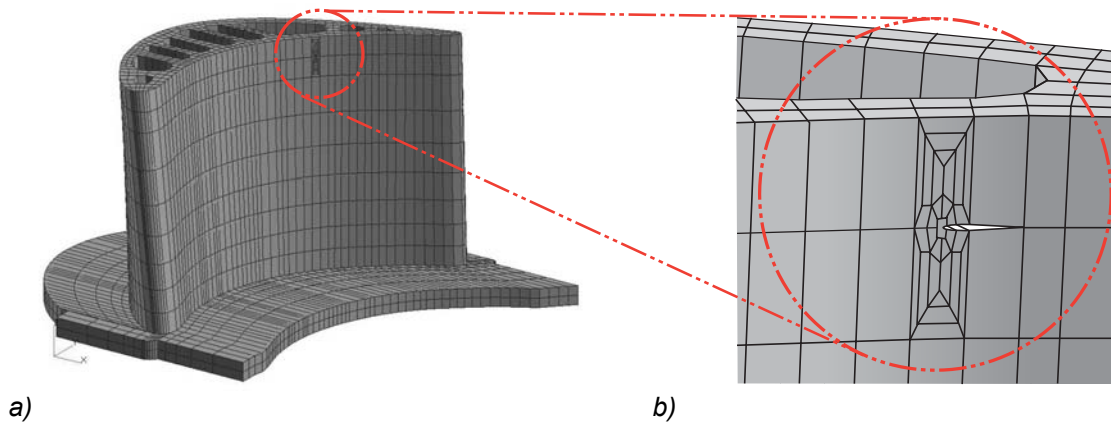


Figure 14 High pressure turbine blade finite element model (lower half shown) and detail of inserted crack

The second example is an FE model of a high pressure turbine blade. A 1.4 mm through crack was inserted in the high pressure turbine blade model.

Figure 14a) using the in-house tool *NLR-C3D* [13], as is shown in

Figure 14b). The stress intensity factors K_I , K_{II} and K_{III} were calculated for five different load cases, using combinations of centrifugal loads, pressure loads and tip rubbing loads. This resulted in five quite different stress states at the location of the crack.

Also, the stress distribution in the uncracked model was calculated for the same five load cases. Since in this case the crack is relatively small and the loading in the region of the crack is rather uniform, again the engineering approach as mentioned above is followed. This means that no influence coefficients were calculated, but one of the elements in the *uncracked* model was assumed to be representative for the loading of the crack. The 3D stress tensor in one of the four elements that were later replaced by crack blocks was transformed to an element local coordinate frame aligned with the crack coordinate frame as defined in Figure 1.

The three stress intensity factors were plotted versus the stress tensor component that is representative for the loading mode (see equation (8)) in Figure 15. This shows that the value of the stress intensity factors is proportional to the stress component across the range of load cases. The correlation for K_{III} is not as good as for K_I and K_{II} , owing to the low relative values of K_{III} making the calculation of K_{III} less accurate. The very strong correlation between K and the corresponding stress component shows again that the SIF solution can be scaled by the three stress components for any stress state and that the selected element in the uncracked model is the appropriate location for the stress tensor to be used for scaling.

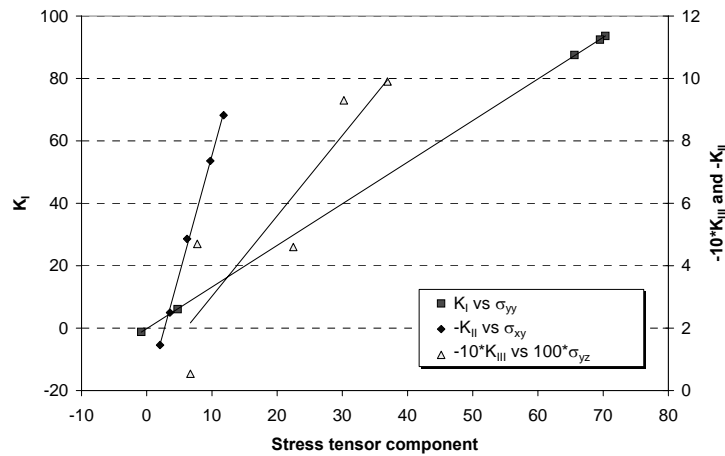


Figure 15 Stress intensity factors plotted versus the stress component that is representative or the loading mode

5.3 Crack propagation analysis method for single crystal gas turbine components

Based on the considerations in the previous subsections a method for crack propagation analysis is proposed consisting of the following steps. The stress intensity factor solution is calculated for a real component for an arbitrary load case using the finite element method. The load sequence for the crack propagation analysis is calculated by performing a fully thermo-mechanical finite element analysis on the uncracked model using a representative load history. Then a representative (effective) stress tensor is calculated by using the influence function method and is used to normalise and scale the SIFs. This yields the values of K_I , K_{II} and K_{III} at any moment in the load history. The tool that was described in the first part of this paper is then used to transform the values of K_I , K_{II} and K_{III} to a value of K_{RSS} . Finally, the sequence of K_{RSS} is used together with the material crack growth data and an appropriate crack growth model to calculate the crack propagation.

This results in a fast and efficient analysis method that combines the benefits of a separated analysis using a closed form stress intensity factor solution with the versatility and ability to include load redistribution effects of (integrated) FE or BE approaches.

6 Concluding remarks

This study has shown that for single crystals of a nickel-base superalloy, CMSX-4, it is inappropriate to use isotropic stress intensity factor solutions, and also projected crack lengths for angled cracks. However, anisotropic stress intensity factor solutions incorporated into a 3-dimensional stress tensor reconstruction, followed by calculations of the resolved shear stress intensity factor, K_{RSS} , gave predictions that explain the fatigue crack growth behaviour in single crystal CMSX-4 corner cracked specimens.

The approach in the present work is based on finite element analyses. This means that it can be extended to the more complex geometries of actual gas turbine components (single crystal turbine blades and vanes). An efficient crack propagation method is proposed, based on the calculation of a closed form stress intensity factor solution and K_{rSS} .

7 Acknowledgements

The author acknowledges the Dutch Ministry of Defence for funding this research under contract NTP N02/12, and J. Botma for the finite element calculations.

8 References

- [1] Telesman J. and Ghosn L. J. The unusual near-threshold FCG behaviour of a single crystal superalloy and the resolved shear stress as the crack driving force. *Engineering Fracture Mechanics* 1989;34(5/6):1183-1196.
- [2] Chan K. S. and Cruse T. A. Stress intensity factors for anisotropic compact-tension specimens with inclined cracks. *Engineering Fracture Mechanics* 1986;23(5):863-874.
- [3] Chen, Q. and Liu, H. W. Resolved shear stress intensity coefficient and fatigue crack growth in large crystals. CR-182137 NASA, 1988.
- [4] Reed, P.A.S., Wu, X.D., Sinclair, I., Fatigue crack path prediction in UDIMET 720 nickel-based alloy single crystals. *Metallurgical and Materials Transactions A* 2000;31A:109-123.
- [5] Labossiere, P.E.W., Dunn, M.L., Calculation of stress intensities at sharp notches in anisotropic media. *Engineering Fracture Mechanics* 1998;61:635-654.
- [6] Zhao, J., Wu, X., Liu, R., Zhang, Z. Finite element analysis of a notch root semi-elliptical crack in single crystal superalloy. *Engineering Fracture Mechanics* 2004;71:1873-1890.
- [7] Courtin, S., Gardin, C., Bezine, G., Ben Hadj Hamouda, H. Advantages of the J-integral approach for calculating stress intensity factors when using the commercial finite element code ABAQUS. *Engineering Fracture Mechanics* 2005;72:2174-2185.
- [8] Sha, J.B., Sun, J., Deng, Z.J., Zhou, H.J. Micro-crack tip fracture of commercial grade aluminium under mixed mode loading. *Theoretical and Applied Fracture Mechanics* 1999;31:119-130.
- [9] Sih G. C., Paris P. C. and Irwin G. R. On cracks in rectilinearly anisotropic bodies. *International Journal of Fracture Mechanics* 1965;1(3):189-203.
- [10] Pickard, A. C. The application of 3-dimensional finite element methods to fracture mechanics and fatigue life prediction. London: Chameleon Press Ltd., 1986.



- [11] Rooke, D. P. and Cartwright, D. J. *Compendium of Stress Intensity Factors*. Uxbridge: The Hillingdon Press, 1976.
- [12] Tada, H., Paris, P. C., and Irwin, G. R. *The stress analysis of cracks handbook*. St. Louis: Del Research Corporation, 1973.
- [13] Tinga, T. *Automatic Stress Intensity Factor calculation using FE methods. Method development and user manual*. NLR-CR-2003-568 Amsterdam: National Aerospace Laboratory, 2003.
- [14] Mom, A. J. A. and Raizenne, M. D. *AGARD engine disc cooperative test programme*. Report no. 766 AGARD, 1989.
- [15] Snyder M. D. and Cruse T. A. *Boundary-integral equation analysis of cracked anisotropic plates*. *International Journal of Fracture* 1975;11 315-328.
- [16] Kolkman, H. J. and Schra, L. *Netherlands contribution to the TA31+/CARAD programme; Fatigue crack growth behaviour of single crystal alloy CMSX4*. NLR-CR-2003-472 Amsterdam: National Aerospace Laboratory, 2003.
- [17] Timbrell, C., Chandwani, R. and Cook, G. *State of the art in crack propagation, Les méthodes de dimensionnement en fatigue*, Journée scientifique du 27 octobre 2004.
- [18] Shiratory, M., Miyoshi, T., Yu, Q., et al., *Development of a software system estimating stress intensity factors and fatigue crack propagation for three-dimensional surface cracks by an influence function method*. *Computer Technology, ASME PVP* 1999;385:299-309.
- [19] Yamashita, Y., Shinozaki, M., et al., *Fatigue crack growth life prediction for surface crack located in stress concentration part based on the three-dimensional finite element method*. *J. Engng Gas Turbines & Power* 2004;126:160-166.